

Li insertion in ball-milled graphitic carbon studied by total x-ray diffraction

This article has been downloaded from IOPscience. Please scroll down to see the full text article.

2011 J. Phys.: Condens. Matter 23 435003

(<http://iopscience.iop.org/0953-8984/23/43/435003>)

View [the table of contents for this issue](#), or go to the [journal homepage](#) for more

Download details:

IP Address: 141.209.165.189

The article was downloaded on 30/09/2011 at 13:27

Please note that [terms and conditions apply](#).

Li insertion in ball-milled graphitic carbon studied by total x-ray diffraction

Valeri Petkov¹, Adam Timmons^{2,5}, John Camardese³ and Yang Ren⁴

¹ Department of Physics, Central Michigan University, Mount Pleasant, MI 48858, USA

² GM Global Vehicle Engineering, Warren, MI 48090, USA

³ Lawrence Technological University, Southfield, MI 48075, USA

⁴ Advanced Photon Source, Argonne National Laboratory, Argonne, IL 60439, USA

E-mail: petkov@phy.cmich.edu

Received 28 May 2011, in final form 30 August 2011

Published 29 September 2011

Online at stacks.iop.org/JPhysCM/23/435003

Abstract

Ball-milled graphitic carbon, both not and electrochemically lithiated, has been studied by total x-ray diffraction involving high-energy synchrotron radiation scattering and atomic pair distribution function analysis. The experimental data has been used to guide reverse Monte Carlo simulations of the three-dimensional structure of the not-lithiated samples.

Experimental and modeling results show that ball milling for short times breaks the graphitic layers into smaller pieces as well as generates extended atomic vacancies. Those increase the overall ability of the material to accommodate lithium. Ball milling for longer times keeps generating even more atomic vacancies in the graphitic layers. Carbon atoms displaced from the layers, however, move in between the layers, turning heavily ball-milled graphitic carbon into an assembly of almost-fused-together, heavily buckled layers that have an impaired ability to accommodate Li atoms. This helps explain well the initial substantial increase and then decrease in the Li storage capacity of ball-milled graphitic carbon. The study demonstrates the great ability of total x-ray diffraction to provide precise structural information for complex materials that are being increasingly explored for energy applications.

(Some figures in this article are in colour only in the electronic version)

1. Introduction

At present a significant research effort is underway worldwide to find advanced negative electrode materials for Li-ion batteries [1]. Graphitic carbon is a material of great interest because it can accommodate Li atoms fast, reversibly and without generating much mechanical stress. In normal conditions pristine graphitic carbon can accommodate up to one Li atom per six carbon atoms. As illustrated in figure 1 the process involves insertion of Li atoms in between the graphitic layers and changing their hexagonal-close-packed ABABAB sequence into an AAAAAA stacking sequence. Due to steric constraints Li atoms can occupy the space above and below the center of only every third hexagonal ring in the graphitic layers resulting in an overall chemical composition of LiC₆ yielding a charge (Li⁺) storage capacity

of 372 mA h g⁻¹ [2]. Real-life applications, however, demand higher Li storage capacities and scientists have been looking into ways to go beyond what bulk LiC₆ can offer. Studies have shown that stacks of graphene sheets [3, 4], nanosized ribbons [5] and carbon nanotubes [6] can store up 2–3 times more Li than bulk graphitic carbon. Although very attractive, nanosized sheets, ribbons and tubes are still too expensive for large-scale industrial applications. That is why other, not so sophisticated but technology more friendly, routes such as ball milling are being explored as well. It has been found that ball-milled graphitic carbon show increased Li storage capacity [7]. The increase has been explained in terms of the ‘stacks of fallen cards’ model (see figure 2) which features breaking, upon the impact of ball milling, of the extended graphitic layers into smaller pieces that are randomly oriented with respect to each other, thus posing a diminished steric hindrance for Li to intercalate. The increased Li storage capacity, however, has been found to fluctuate with the milling

⁵ Currently with Chrysler Corporation, Auburn Hills, MI 48326, USA.

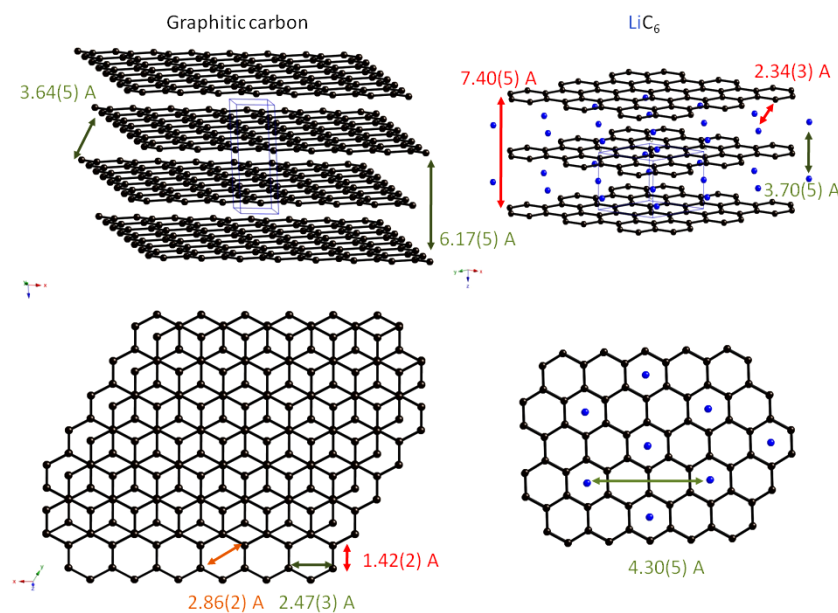


Figure 1. Fragments of the crystal structures of graphite (left) and LiC_6 (right). The respective unit cells are outlined with thin lines (in blue). Lateral view of the structures is shown in the upper part of the plot and a top view in the lower. Several interatomic distances between carbon (circles in black) and Li (circles in blue) atoms are marked with arrows. Note the packing sequence of the graphitic layers changes from ABABABA to AAAA type upon Li intercalation.

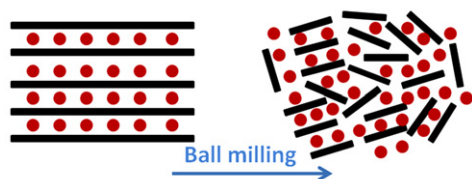


Figure 2. ‘Stack of fallen cards’ model for ball-milled graphitic carbon (black bars) loaded with Li atoms (red dots).

time, puzzling scientists for more than a decade. Here we address this problem by determining the exact atomic-scale structure state of a series of ball-milled graphitic carbon which show a great variation in their Li storage capacity. The structure determination is done by total x-ray diffraction (XRD) [8, 9] which has recently proven to be very efficient in the case of fine powders, including those obtained by ball milling [10, 11].

2. Experimental details

2.1. Ball-milled sample preparation and characterization

Natural flake graphitic carbon (Alfa Aesar, 99.995% pure) was milled for 10, 70, 150, 310 and 1270 min using a SPEX 8000D mill with a shaking frequency of 1400 RPM. The milling was done at room temperature in ambient air, in Ar gas atmosphere and in a mixture of Ar with 5 vol% H_2 gas atmosphere. Here results for graphitic carbon milled in air are shown and discussed only since this material showed the best Li storage capacity properties. The chemical composition of the fine powders resulting from the ball milling was checked by electron probe microanalysis. No

substantial contamination from the steel grinding vial and ball bearings was found. Figure 3 shows scanning transmission electron microscopy (STEM) images, taken with a JEOL JSM-840A instrument, of particles of the pristine graphitic and ball-milled carbon powders. The powders were also characterized by Raman spectroscopy using a 5000 series Hololab Raman instrument equipped with a laser source with a wavelength of 785 nm. Figure 4 shows the respective spectra. The surface area of the samples was estimated within the Brauner–Emmett–Teller (BET) model framework using N_2 gas adsorption and a Quantachrome Autosorb 1 instrument. Figure 5 shows the results from the surface area measurements.

2.2. Sample lithiation and Li storage capacity measurements

Pristine graphitic carbon and ball-milled graphitic powders were electrochemically loaded with lithium (i.e. lithiated) inside of a glove box in an inert Ar gas atmosphere. Each powder sample was individually wrapped with sheets of brushed lithium metal foils that were perforated to facilitate the electrolyte access. The electrolyte was composed of 1 M LiPF_6 salt dissolved in a 1:2 volume mixture of ethylene carbonate (EC) and diethyl carbonate (DEC) solvents. After 24 h of lithiation the samples, still inside the glove box, were sealed into glass capillaries suitable for x-ray diffraction experiments. It was expected that the surface of the thus lithiated carbon powder particles would be covered by an electrolyte reduction product, precipitated LiPF_6 salt and EC solvent, which is solid at room temperature when not mixed with another solvent. Therefore, a sample of the electrolyte after the DEC was evaporated, leaving only precipitated LiPF_6 salt and solid EC, was also prepared. It was used to estimate

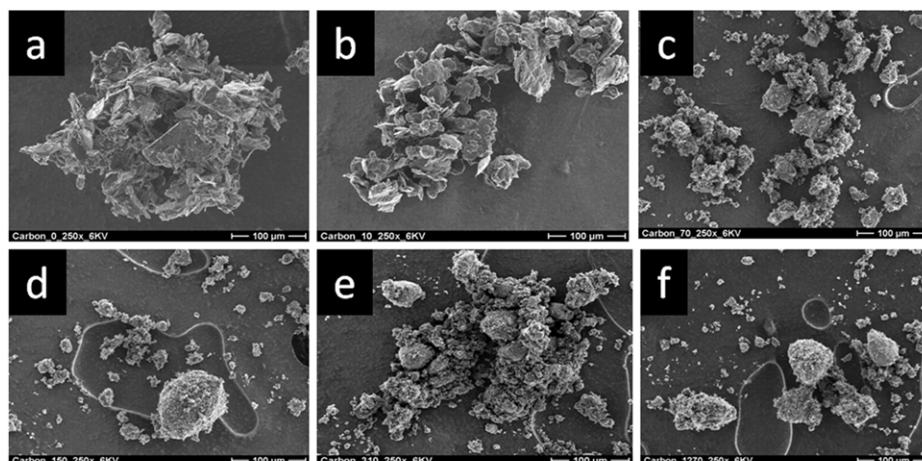


Figure 3. STEM images of pristine graphitic carbon (a) and carbons ball-milled for 10 min (b), 70 min (c), 150 min (d), 310 min (e) and 1270 min (f). Transparent contour loops in ((c)–(f)) come from irregularities of the Al sample holder used in the STEM instrument.

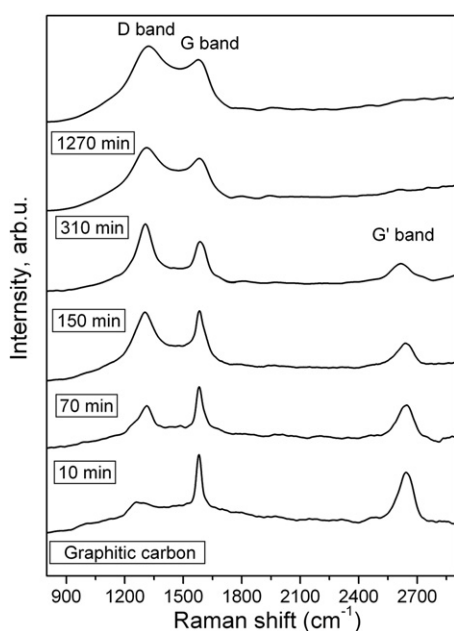


Figure 4. Raman spectra of pristine and ball-milled graphitic carbon powders. Spectra are shifted up by a constant for clarity and marked with the respective milling times (in minutes). The spectra show three major bands: first-order D and G, and second-order G' (also known as D2) bands.

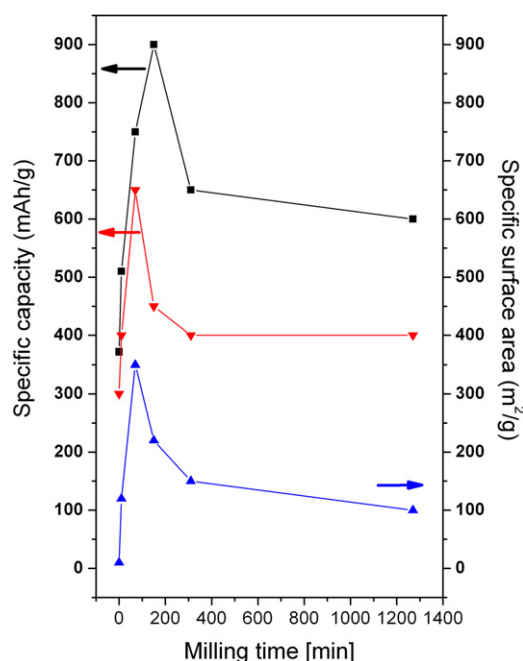


Figure 5. Recoverable (squares/black) and non-recoverable (down triangles/red) Li storage capacity in ball-milled graphitic carbons (axis on the left). BET surface area data (up triangles/blue) are shown as well (axis on the right).

the contribution of the precipitated LiPF_6 salt and solid EC alone to the experimental XRD data.

The Li storage capacities were measured by collecting potential (i.e. voltage) and current data of a half-cell with composite electrodes made of the lithiated carbon powders and copper foil substrates. At first the half-cell was fully discharged at a constant rate of C/10, i.e. for 10 h, until it reached a potential of 0.001 V versus Li/Li^+ . The cell was held at this potential until the current reached 1/8 of the value defined by the C/10 rate. Then, the half-cell was charged at a constant C/10 rate until the potential reached a value of 2.5 V versus Li/Li^+ . This was followed by a

30 min period of open circuit. The process was repeated several times at C/20, C/30, etc. rates until the cell completed a charge at a constant rate of C/80. Subsequently, the cell was again discharged. The recoverable, also called reversible, Li storage capacity was calculated from the integral of current and time during the second complete discharge, divided by the mass of the active material in the composite electrode of the half-cell. The non-recoverable, approximately equal to the so-called irreversible Li storage capacity was obtained from the difference in the storage capacity values of the first and second complete discharges. Figure 5 shows the as-obtained recoverable and non-recoverable Li storage capacity data.

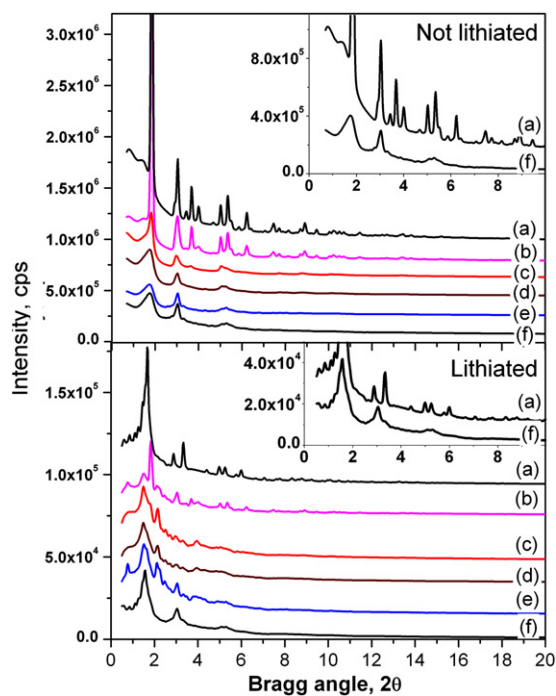


Figure 6. Synchrotron XRD patterns for not and electrochemically lithiated graphitic carbon in pristine state (a) and ball-milled for 10 min (b), 70 min (c), 150 min (d), 310 min (e) and 1270 min (f). The low-angle part of the XRD patterns for the not-milled and 1270 min milled samples are given in the insets.

2.3. High-energy x-ray diffraction measurements

X-ray diffraction experiments were carried out at the 11-IDC beamline at the Advanced Photon Source using x-rays with energy of 115.232 keV ($\lambda = 0.1076 \text{ \AA}$) and a large-area (mar345) detector. Synchrotron radiation x-rays were used for two reasons. Firstly, the higher flux of synchrotron radiation x-rays makes it possible to measure the rather diffuse diffraction patterns of ball-milled graphitic powders with a very good statistical accuracy. Secondly, the higher energy of synchrotron radiation x-rays makes it possible to reach higher wavevectors, Q , which is vital for the atomic pair distribution function (PDF) analysis [8–11] performed here. Both not-lithiated and lithiated samples, all sealed in glass capillaries, were measured. Up to ten exposures were taken for each of the samples, and each exposure lasted 10 min. The experimental XRD patterns are shown in figure 6.

3. Results

As can be seen in figure 3(a) the primary particles of pristine graphitic carbon have a platelet-type morphology reflecting its layered-type (see figure 1, left) atomic-scale structure. Those platelets are several tens of microns across and progressively get smaller in size when ball-milled for 10–70 min (see figures 3(b) and (c)). At longer milling times, 150 min and longer, some of the already smaller size platelets are seen to start coalescing into a new type of primary particles of oval shape (see figure 3(d)) whose size approaches that of

the original platelets. Carbon milled for more than 150 min contains quite a few oval particles that tend to agglomerate together (e.g. see figure 3(f)). Materials made of particles of smaller size have an extended surface area and vice versa. STEM images thus indicate that graphitic carbon ball-milled for up to 70 min would have a larger surface area than the pristine (i.e. not milled) graphitic carbon. The surface area of carbon milled for longer times would then start to decrease because of the coalescing of the smaller platelets into larger size oval particles. Our BET surface area data (see figure 5) and results of others [12] show that it is indeed the case. From all carbon samples studied here, the one milled for 70 min has the largest specific surface area of approximately $350 \text{ m}^2 \text{ g}^{-1}$. The progressively changing morphology of ball-milled carbon also affects their XRD patterns. Figure 6 (upper part) shows that the XRD pattern of pristine graphitic carbon has several sharp Bragg peaks as it should be for a micron-sized crystalline material. The peaks are getting progressively broader with milling times to a state where they merge into a few broad humps in the diffraction pattern for 1270 min milled carbon. Bragg peak broadening may come from smaller crystallite sizes, increased lattice strain and/or the presence of a substantial number of structural defects. The first, i.e. a decrease in the crystallite's size, does occur in the ball-milled samples as the STEM and BET data show. According to our Raman results (see figure 4) the latter also occur in ball-milled carbon. Pristine graphitic carbon shows two strong Raman lines at approximately 1587 and 2640 cm^{-1} . They are due to first- and second-order Raman scattering and called G and G' bands, respectively [3, 13, 14]. Structural defects are known to break down the hexagonal symmetry of the graphitic carbon, modify the optical selection rules of the cooperative atomic vibrations, induce an additional Raman line, the so-called D band at approximately 1360 cm^{-1} , and reduce the intensity of the G' band [3, 13, 14]. The Raman spectra of ball-milled carbon exhibit both the G and D bands, with the intensity of the latter increasing with milling time. At the same time the G' band is seen to gradually disappear with increasing milling time. Obviously not only the morphology/particle size but also the hexagonal-type atomic ordering within the layers of the graphitic carbon is substantially modified by the milling process. Traditional XRD, spectroscopy like Raman and imaging techniques like STEM, however, are not able to reveal the exact nature of this modification. The same is true for the lithiated samples. Their XRD patterns are also very diffuse in nature, especially those for the samples obtained by ball milling for longer times (see figure 6, lower part). To reveal the nature of the atomic ordering in both the as-made and then lithiated ball-milled carbon we analyzed the XRD data in terms of their Fourier counterparts, the so-called atomic PDF functions. The advantage of the PDF analysis is that it takes into account both the Bragg-like and diffuse components of the diffraction data. In this way both the longer-range atomic ordering, manifested in the Bragg-like peaks, and the structural imperfections, manifested in the diffuse component of the diffraction pattern, are reflected in the PDF. Besides, atomic PDFs are less affected by diffraction

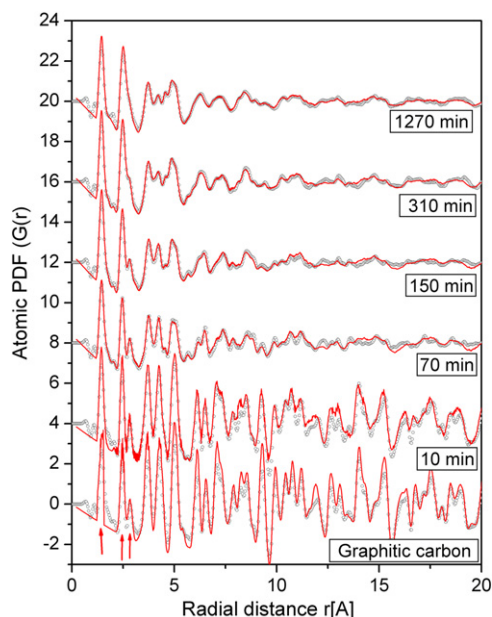


Figure 7. Experimental (symbols) and model (full line) atomic PDFs of pristine and ball-milled graphitic carbon. PDFs are shifted up by a constant for clarity and marked with the respective milling times (in minutes). The model PDFs are computed from RMC-constructed 60 000-atom configurations. Arrows mark the three shortest distances, 1.42 Å, 2.47 Å and 2.86 Å, respectively (see figure 1, left), in graphitic carbon. Note the experimental PDF data for the milled samples do not show any detectable signature of a second (e.g. oxygen- or metal-containing) phase.

optics and experimental factors since these are accounted for in the step of reducing the XRD data into PDFs [8–11]. This renders the PDF a structure-dependent quantity that directly reflects the relative positions of atoms in materials, i.e. a quantity that is very suitable for testing and refining of structural models. Figures 7 and 8 show the atomic PDFs $G(r)$ for not and lithiated ball-milled carbon, respectively. The reducing of the experimental XRD data into atomic PDFs was done with the help of the program RAD [15].

4. Discussion

Peaks in atomic PDFs occur at distances separating well-defined atomic pairs. In particular, the first PDF peak in all carbon samples shown in figure 7 is positioned at a distance of 1.42 Å, which is the first neighbor (sp^2) carbon–(sp^2) carbon distance in graphite. The PDF for the pristine (i.e. not milled) graphitic carbon shows many more well-defined peaks extending to long interatomic distances (see figure 7). All peaks can be very well approximated with a model based on the structure of crystalline graphite shown in figure 1 (left). The good agreement between the model computed and experimental data attests to the good quality of the present high-energy XRD experiments and subsequent data reduction into atomic PDFs. The PDF for the lithiated pristine graphitic carbon also shows very well-defined peaks extending to long interatomic distances (see figure 8) indicating that this material, like pristine graphitic carbon, is crystalline in nature.

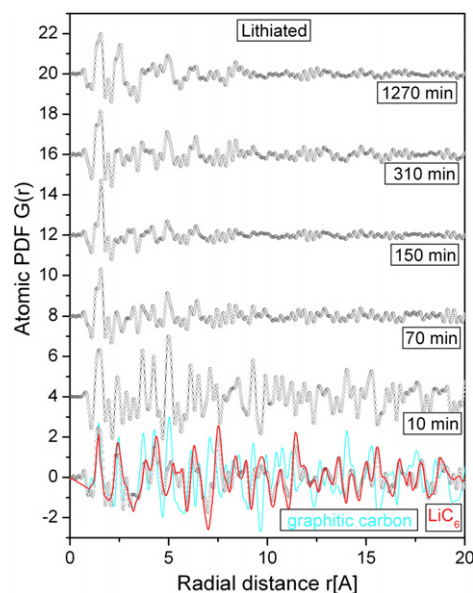


Figure 8. Experimental atomic PDFs (symbols) of electrochemically lithiated pristine and ball-milled graphitic carbon. PDFs are shifted up by a constant for clarity and marked with the respective milling times (in minutes). The experimental PDF for the lithiated pristine sample is fitted very well with a model PDF (line in red/gray) computed from the crystal structure of LiC_6 . The experimental PDF for the not-lithiated pristine carbon (line in cyan/light gray) is shown as well. Beyond the first three PDF peaks it oscillates differently from the way the PDF for the respective lithiated sample does, reflecting the different packing sequences (see figure 1) of the graphitic layers in the two materials.

In this case the experimental PDF data are every well approximated by a model based on the structure of crystalline LiC_6 shown in figure 1(right). Obviously the electrochemical lithiation has been completed close to its full extent under the experimental conditions (room temperature and normal pressure) adopted by us. This is also confirmed by the respective experimental Li storage capacity data which is very close (see figure 5) to the expected value for LiC_6 of 372 mAh g^{-1} . Note that not fully loaded with Li graphitic carbon has an atomic-scale structure and Li storage capacity very different from that of LiC_6 [2, 16]. The experimental PDF for the sample milled for 10 min is very similar to that of the not-milled one (see figure 7), indicating that short milling times hardly affect the atomic-scale structure of graphitic carbon, except for breaking the graphitic layers into smaller pieces (e.g. compare the images in figures 3(a) and (b)). Milling for longer times, however, affects it considerably since the PDF peaks, i.e. the atomic coordination spheres they reflect, start losing their sharpness leading to a reduction of the length of structural coherence, measured by the real space distance at which the PDF data decay to zero, to only 20–30 Å. Indeed the atomic PDFs for graphitic carbon milled for 70–1270 min resemble very much those of low crystallinity carbon obtained by a thermal decomposition of organic precursors [17, 18]. The graphitic planes in those low crystallinity carbon are found to be rich in structural defects and heavily buckled [17]. A careful analysis of the experimental data in figure 7 indicates that this may be

the case with graphitic carbon ball-milled for longer (than 70 min) times. In particular, the second (2.47 Å) and third (2.86 Å) PDF peaks (marked with arrows in figure 7) are seen to progressively broaden with milling time and merge into a single peak in the PDF for the sample milled for 1270 min. The second and third PDF peaks reflect the correlations between the second and third carbon–carbon atomic neighbors within the hexagons of graphitic layers (see figure 1, left). The broadened distribution of these correlations/distances, given the well-preserved first-neighbor correlation/distance of 1.42 Å (see figure 7), indicates that with milling time carbon atoms become progressively displaced from the graphitic layers, i.e. that the latter progressively lose their flat-plane character. The lithiation does not seem to change the structurally disordered nature of carbon milled for more than 10 min. Figure 8 shows that the respective atomic PDFs exhibit only a few peaks at low (up to 10–15 Å) distances.

To understand the atomic-scale structure of ball-milled carbon in more detail we constructed three-dimensional (3D) structural models using the experimental PDF data as a guide. The models were generated by reverse Monte Carlo simulations (RMC) that are capable of building large size, and so statistically very representative, atomic configurations. In brief, the RMC simulations start with the creation of a model atomic configuration which is positioned inside a simulation box. The configuration is tested and, if found consistent, further refined against the experimental PDF data. The refinement is done by varying the coordinates of the atoms from the model atomic configuration in a random manner so as to obtain the best possible agreement between the experimental and model computed PDF [19, 20]. We started with a configuration of 60 000 atoms arranged as in graphite (see figure 1, left). That model converged immediately, reproducing the experimental data for the not-milled sample very well. The resultant configuration was used as a starting point in the modeling of the 10 min milled sample structure. Following the same feed-forward strategy the structures of the samples milled for 70, 150, 310 and 1270 min were modeled. The simulations were done with the help of the computer program RMC++ [21] and run until the respective experimental PDFs were reproduced in finest detail (see figure 7). Representative fragments of the final atomic configurations are shown in figure 9.

As can be seen in figure 9(a) that the graphitic layers are perfect and well lined up in an ABABAB sequence in the not-milled samples studied by us. Carbon atoms in the 10 min milled sample (figure 9(b)) are somewhat displaced out of the originally perfectly flat graphitic layers. Some missing atom-type vacancies appear on the layers as well. With the samples milled for longer times more and more carbon atoms move further and further out of the graphitic layers opening extended missing atom-type vacancies on them (see figures 9(c) and (f)). These atomic displacements are quite uncorrelated making the graphitic layers look like locally swelled to various degrees. Some of the atoms displaced from the layers end up trapped in between the layers, turning the carbon milled for 310 and 1270 min into an assembly

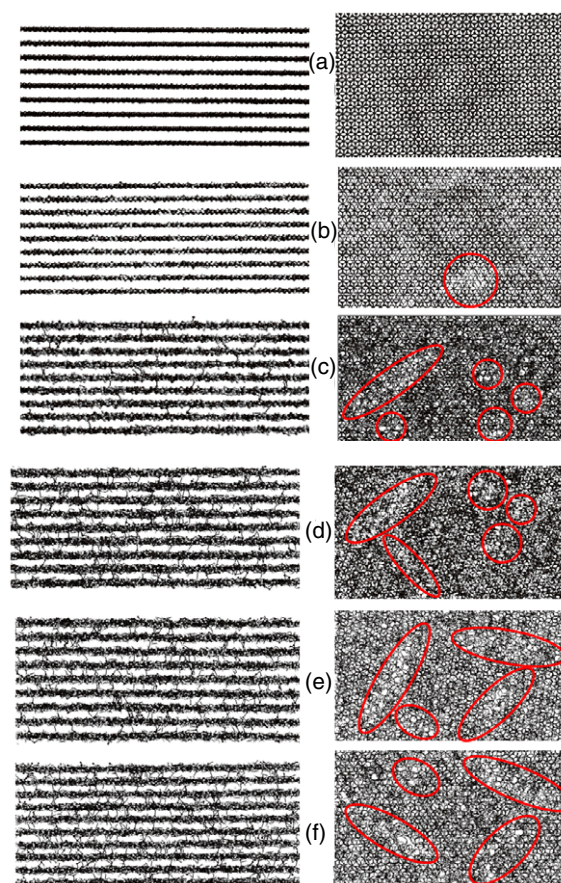


Figure 9. Fragments of the RMC constructed models of graphitic carbon (lateral view left and top view right) in pristine state (a) and ball-milled for 10 min (b), 70 min (c), 150 min (d), 310 min (e) and 1270 min (f). Circles and ellipses (in red) mark the extended planar defects (missing atoms) in the graphitic planes of the ball-milled samples.

of heavily distorted (out-of-plane), defective (missing atoms) and locally fused together graphitic layers. Other studies [13] have also suggested the possibility that some carbon atoms may end up ‘intercalated’ in between the graphitic layers of ball-milled carbon. Our study provides clear evidence that this is indeed the case. With these findings at hand the Li storage capacity properties of ball-milled graphitic carbon are easier to explain. To do it we concentrate on the low- r part of the atomic PDFs for the lithiated samples shown in figure 10. The experimental atomic PDF for the precipitated electrolyte alone is shown in this figure as well. The precipitated electrolyte is expected to be very similar in nature to the electrolyte decomposition phase forming on the surface of the carbon particles during their electrochemical lithiation. As can be seen in figure 10 the precipitated electrolyte phase is very disordered structurally, i.e. is in an amorphous state, having only one very well-defined interatomic correlation/first coordination sphere positioned at approx. 1.65 Å. That interatomic correlation explains the right-hand shoulder of the first PDF peak in the lithiated pristine graphitic carbon. The other peaks in the atomic PDF for this not-milled sample are very well explained by a model based on the structure of LiC_6 (also see figure 8). Obviously

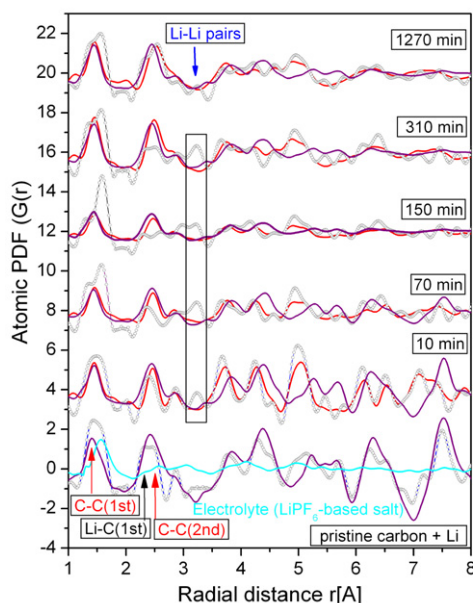


Figure 10. Low- r part of the experimental atomic PDFs (symbols) of electrochemically lithiated pristine and ball-milled graphitic carbon and the polyelectrolyte (line in cyan/light gray) used in their preparation. PDFs are shifted up by a constant for clarity and marked with the respective milling times (in minutes). Also shown are the model PDFs (line in red/gray) for the milled but not lithiated samples (same as in figure 7). Model PDFs (line in brown/dark gray) computed from a progressively disordered LiC_6 crystal model are shown as well. Arrows mark the position of several atomic pair correlations.

Li fully loaded pristine graphitic carbon material is a phase mixture of a bulk LiC_6 and a surface, electrolyte-based phase, with the former being a major reversible storage place for the Li atoms since the measured Li storage capacity is very close to that (see figure 5) of LiC_6 . As can be expected, the contribution of the surface, electrolyte-based phase to the experimental PDF data is seen (see the behavior of the right-hand shoulder of the first peak in the atomic PDFs shown in figure 10) to correlate with the specific (BET) surface area of the respective carbon particles. It becomes more substantial for the carbon milled for 10–70 min that have an increased surface area as compared to the pristine graphitic carbon (see figure 5) and then drops with the longer-times milled carbon that has a decreased specific surface area (see figure 5). It is believed [22, 23] that the surface, electrolyte-based phase is where Li may get trapped, i.e. lost for battery-related applications requiring fast and recoverable Li loading/charging and draining/discharging. Our data for the non-recoverable Li storage capacity (see figure 5) nicely correlate with the amount of the surface, electrolyte-based phase revealed by the experimental PDF data. Both initially increase, reach a maximum for the sample milled for about 70 min and then sharply decrease.

A careful analysis of the PDF peaks pertaining to the carbon particles then allows us to understand the recoverable Li storage capacity data. In particular, the second peak in the PDFs shown in figure 10 has contributions (marked with

arrows) coming from first-neighbor Li–C atomic correlations (2.35 Å) within the LiC_6 -type structure and C–C atomic correlations (2.47 Å) from the hexagons of the graphitic layers. The Li–C correlations are very well expressed in the not-milled and in the samples milled for 10, 70 and 150 min. Then they start fading away, making the C–C correlation at 2.47 Å dominant in the sample milled for 1270 min. Indeed the PDF for the 1270 min milled sample is much better explained by a model based on not-lithiated, heavily disordered carbon (red line in figure 10) than a model based on fully Li loaded, i.e. LiC_6 -type, graphitic carbon (brown line in figure 10). Obviously a good fraction of the graphitic carbon milled for longer (than 150 min) times do not accommodate as much Li as graphitic carbon milled for shorter (than 150 min) times. Instead, they retain the ABABAB-type sequence of distorted graphitic layers, i.e. are lost for battery applications. The reason for this behavior lies in the heavily distorted structure of such carbon. Their graphitic layers are not flat but locally buckled and even fused together (see figures 9(e) and (f)) which may easily frustrate the Li intercalation process.

5. Conclusions

Results from the present study show that the ‘stack of fallen cards’ model is valid for graphitic carbon milled for only very short times. The graphitic planes in such carbon do brake into smaller pieces (see figures 3(a)–(c)) and, to a great extent, remain rather flat (see figures 9(a)–(c)). Accordingly Li atoms can easily be accommodated in between the layers, at the edges of smaller size layers and at defect sites within the layers (see figure 9, right). There are no strong steric constraints for the Li atoms at the edges and vacancies within the layers so that the former may come together closer than in the bulk LiC_6 phase where the Li–Li atomic pairs are separated at distances from 3.7 Å (in a direction perpendicular to the layers, see figure 1, right) to 4.3 Å (in a direction along the layers) [2]. The experimental PDF data indicate that pairs of Li atoms separated at distances of approximately 3.2 Å may form in graphitic carbon ball-milled for 10–310 min (see figure 10). Notably, this is the distance between Li atoms in Li metal [24]. Li atoms at the edges and defects within the graphitic layers are in excess of what the bulk LiC_6 -type phase can store and so the overall recoverable Li storage capacity increases from 372 mA h g^{-1} in the not-milled graphitic carbon to almost 900 mA h g^{-1} in graphitic carbon milled for 150 min (see figure 5). The graphitic layers in carbon milled for longer times, however, become too buckled and locally fused together (see figures 9(e) and (f)), making it increasingly difficult for Li to intercalate in between them. Furthermore, the broken and heavily deformed graphitic platelets agglomerate in larger particles (see figures 3(e) and (f)), eventually blocking the access of Li to their interior which thus does not turn into an LiC_6 phase but remains an ABABAB-type pure graphitic phase (see the PDFs in figure 10). As a result the overall recoverable Li storage capacity decreases from its maximal value (see figure 5). To increase this value further other technological routes that not

only yield very fine size graphitic platelets but also retain their out-of-plane structural integrity have to be explored. Care should also be exercised to optimize their surface area so that the non-recoverable Li storage capacity is kept to a minimum.

On a more general note, fine powder materials will continue to be explored as negative and positive electrode active materials in battery-related applications. The present study demonstrates that total XRD can provide very precise structural information for lithiated carbon-based materials used as negative electrodes. Our earlier studies [25] demonstrated that total XRD is also very useful in studying lithiated fine powder transition-metal oxides used as positive electrode active materials. Total XRD is very useful in studying organic-inorganic composites [26] as the blends of negative electrode/polyelectrolyte/positive electrode in batteries are in fact. The technique requires a small amount of sample and can work in different environments. It has the potential of becoming a major structure determination tool in studies on materials explored for batteries and other energy-related applications.

Acknowledgments

Work at APS was supported by DOE under contract DE-AC02-06CH11357. The authors are indebted to B Pavan and G Garabedian for the help with the Raman and BET experiments, respectively.

References

- [1] Wagner T F, Lakshmanan B and Mathas M F 2010 *J. Phys. Chem. Lett.* **1** 2204–19
- [2] Guerard D and Herold A 1975 *Carbon* **13** 337–45
- [3] Pan D, Wang S, Zhao B, Wu M, Zhang H, Wang Y and Jiao Z 2009 *Chem. Mater.* **21** 3146–2
- [4] Yoo E, Kim J, Hosono E, Zhou H-S, Kudo T and Honma I 2008 *Nano Lett.* **8** 2277–82
- [5] Bhardwaj T, Antic A, Pavan A, Barone V and Fahlman B D 2010 *J. Am. Chem. Soc.* **132** 12556–1258
- [6] Shimoda H, Gao B, Tang X P, Kleinhannes A, Fleming L, Wu Y and Zhou O 2002 *Phys. Rev. Lett.* **88** 015502
- [7] Disma F, Aymard L, Dupont L and Tarascon J M 1996 *J. Electrochem. Soc.* **143** 3959–72
- [8] Egami T and Billinge S J L 2003 *Underneath the Bragg Peaks* (Amsterdam: Pergamon)
- [9] Petkov V 2008 *Mater. Today* **11** 28–38
- [10] Gateshki M, Petkov V, Williams G, Pradhan S K and Ren Y 2005 *Phys. Rev. B* **71** 224107
- [11] Gateshki M, Petkov V, Pradhan S K and Vogt T 2005 *J. Appl. Crystallogr.* **38** 772–9
- [12] Chen Y, Gerald J F, Chadderton L T and Chaffron L 1999 *Appl. Phys. Lett.* **74** 2782–4
- [13] Wang C S, Wu G T and Li W Z 1998 *J. Power Sources* **76** 1–10
- [14] Pimenta M A, Dresselhaus G, Dresselhaus M S, Cancado L G, Jorio A and Saito R 2007 *Phys. Chem. Chem. Phys.* **9** 1276–91
- [15] Petkov V 1989 *J. Appl. Crystallogr.* **22** 387–9 available free at: www.phy.cmich.edu/people/petkov/software.html
- [16] Billaud D, McRae E and Herold A 1979 *Mater. Res. Bull.* **14** 857–64
- [17] Petkov V, DiFrancesco R G, Billinge S J L, Acharya M and Foley H C 1999 *Phil. Mag. B* **79** 1519–30
- [18] Oshida K, Nakazawa T, Osawa K and Endo M 2009 *Cent. Eur. J. Phys.* **7** 232–6
- [19] McGreevy R L and Pusztai L 1998 *Mol. Simul.* **1** 359–67
- [20] Dove T M, Tucker M G, Wells S A and Keen D A 2002 *EMU Notes Mineral.* **4** 59–82
- [21] Gereben O, Jóvári P, Temleitner L and Pusztai L 2007 *J. Optoelectron. Adv. Mater.* **9** 3021–7
- [22] Aurbach D, Markovsky B, Weismann I, Levi E and Ein-Eli Y 1999 *Electrochem. Acta* **45** 67–86
- [23] Peled E, Golodinsky D, Ulus A and Yufit V 2004 *Electrochem. Acta* **50** 391–5
- [24] Nadler M R and Kempfer C P 1959 *Anal. Chem.* **31** 2109–11
- [25] Gateshki M, Hwang S-Ju, Park D H, Ren Y and Petkov V 2004 *J. Phys. Chem. B* **108** 14956–63
- [26] Petkov V, Parvanov V, Trikalitis P, Malliakas Ch, Vogt T and Kanatzidis M 2005 *J. Am. Chem. Soc.* **127** 8805–12